RSC Advances

PAPER

View Article Online
View Journal | View Issue

Cite this: *RSC Adv.*, 2021, **11**, 28000

A rapid and simple preparation of amphotericin B-loaded bacterial magnetite nanoparticles†

Tarcisio Correa,[a] Dennis A. Bazylinski,[b] Flávio Garcia [c] and Fernanda Abreu *[a]

Magnetotactic bacteria, which synthesize biological magnetite nanoparticles (BMs), are the main microbial source of magnetic nanomaterials. Although the use of BMs has been explored *in vitro* and *in vivo* for new anticancer formulations, targeted treatments of fungal and parasitic diseases would also benefit from biogenic magnetic nanoformulations. Due to the necessity of new formulations of amphotericin B, we developed a magnetic-nanoparticle based conjugate of this drug using bacterial magnetosomes. Different amphotericin B preparations were obtained using BMs extracted from *Magnetovibrio blakemorei* strain MV-1^T as well as glutaraldehyde and poly-L-lysine as linking reagents. The highest capture efficiencies and drug loadings were achieved using 0.1‰ poly-L-lysine as the only linking agent (52.7 ± 2.1%, and 25.3 ± 1.9 μg per 100 μg, respectively) and 0.1‰ poly-L-lysine and glutaraldehyde 12.5% (45.0 ± 5.4%, and 21.6 ± 4.9 μg per 100 μg, respectively). Transmission electron microscopy and infrared spectroscopy analyses confirmed the association of amphotericin B to the BM surface. Moreover, controlled drug release from these nanoparticles was achieved by applying an alternating magnetic field. In this condition the release of amphotericin B in PBS increased approximately four-fold as compared to the release under standard conditions with no applied magnetic fields. Hence, the functionalization of BMs with amphotericin B produces stable nanoformulations with a controllable drug release profile, thus, enabling its potential in the treatment of fungal and parasitic diseases.

Received 20th May 2021
Accepted 10th August 2021

DOI: 10.1039/d1ra03950d

rsc.li/rsc-advances

Introduction

Magnetic nanoparticles have extensive usage in nanomedicine, mainly because of their employability in drug delivery, biomolecule immobilization, and cell separation.[1] In drug immobilization, nanoparticles lead to the increased biocompatibility of these compounds as they reduce toxic effects by preventing systemic distribution.[1,2] Besides, they drive therapeutic molecules to the site of interest (*i.e.*, site of infection or tumors) leading to a higher local concentration than when using non-immobilized drugs.[2] Several magnetic nanoparticle systems have been developed in the last decades.[1] Most of them comprise synthesis of nanoparticles by precipitation of iron minerals such as magnetite.[1,3] Surface modifications of these nanoparticles are usually performed to make them able to bind to functional moieties.[3] However, processes of chemical synthesis may not yield particles with uniform sizes, and shapes and their magnetic properties are difficult to predict.[4]

Bacterial magnetite nanoparticles (BMs), known as magnetosomes, overcome these limitations.[5] These nanoparticles, which are synthesized in a finely-controlled biomineralization process by magnetotactic bacteria,[6] comprise a core mineral crystal of magnetite or greigite enveloped by a lipid bilayer membrane.[7] Biomineralization process yields single domain magnetic nanoparticles within a narrow size range (30–100 nm) and uniform shape.[8] Further surface modification steps are straightforward because of the natural membrane bilayer of these nanoparticles. Proteins responsible for the magnetosome synthesis are embedded in this outer lipid bilayer,[6] being useful for functionalization processes.[5,10] They can work as anchors for expression genetically-engineered fusion proteins such as enzymes or antibodies.[11,12] Alternatively, their amino groups ($-NH_2$) may serve as sites for crosslinking with other molecules, such as drugs.[13,14]

All those characteristics are advantageous for biomedical applications.[5,8] Additionally, bacterial synthesis of magnetite nanoparticles is considered environmentally friendly.[3,9] Several applications for BMs have been described. In small-molecule immobilization, gangliosides and the antitumor drugs doxorubicin and cytarabine have been surface-bound to BMs and, in all cases, their activities were shown to be enhanced in the magnetic conjugate.[13,15,16] However, all of these tests were performed with highly hydrophilic molecules and both drugs tested were anticancer.[13,15,16]

[a]*Instituto de Microbiologia Paulo de Góes, Universidade Federal do Rio de Janeiro, Avenida Carlos Chagas Filho, 373, CCS, UFRJ, Rio de Janeiro, RJ 21941-902, Brazil. E-mail: fernandaabreu@micro.ufrj.br*

[b]*School of Life Sciences, University of Nevada at Las Vegas, Las Vegas, Nevada, USA*

[c]*Centro Brasileiro de Pesquisas Físicas, Rio de Janeiro, Rio de Janeiro, Brazil*

† Electronic supplementary information (ESI) available: Supplementary Fig. S1–S4. See DOI: 10.1039/d1ra03950d

Unlike the examples above, amphotericin B (AmB) is a poorly water-soluble, antifungal and leishmanicidal drug belonging to polyene class.[17] Because of poor dispersibility in aqueous media and serious toxic side-effects, nanoparticle formulations for this drug could come as beneficial for its therapeutic use.[18–20] Different formulations have been developed for AmB such as Fungizone® and AmBisome®, which are less toxic and disperse well in bodily fluids.[20] Zaioncz *et al.*[21] reviewed several works on AmB formulations using nanoparticles as carriers, including polymeric-based, protein-based, and solid lipid-based nanoparticles, some of the which with more efficacy, bioavailability, and less toxicity than other formulations on market. More recently, a formulation of AmB-loaded polycaprolactone (PCL) was designed for topical treatment with significant lower IC_{50} compared with free AmB and AmBisome®.[22] To benefit from the stimuli-responsiveness of magnetic materials, Niemirowicz and colleagues developed a magnetic nanoformulation that was efficient at inhibiting biofilm formation of *Candida* sp. and increase the antifungal activity of polyene antibiotics, even in resistant *Candida* strains.[23] Nevertheless, the nanoparticle tested was chemically synthesised. The use of BMs for immobilizing AmB could bring additional advantages to magnetic formulations, such as low side-effects, and, additionally, the surrounding biological membrane could facilitate functionalization because of the availability of functional groups on their surface for chemical modification. In addition, AmB biocompatibility and dispersibility would be enhanced.

In the present work, we describe a rapid and simple preparation of BMs–AmB conjugates. The drug was attached to the surface of elongated prismatic BMs from the magnetotactic vibrio *Magnetovibrio blakemorei* strain MV-1^T through crosslinking with glutaraldehyde (GA), coating with poly-L-lysine (PLL) and a combination of both in different concentrations. Finally, we investigate AmB release under standard condition and under application of an alternating magnetic field (AMF).

Experimental

Materials

All reagents used in experiments were purchased from Sigma-Aldrich (St. Louis, MO, USA) with the exception of AmB, that was purchased from Inlab (São Paulo, Brazil). PLL was of a molecular weight range of 70 000–150 000 in a solution at 0.01%.

Bacterial culture

Cells of *Mv. blakemorei* strain MV-1^T were anaerobically cultured in an optimized medium[24] in vials for 48 hours at 28 °C before being used in fermentation experiments.

Bioreactor culture

Volumes corresponding to a final cell concentration of 10^8 cells per mL were inoculated into a 5 L benchtop bioreactor (2 L working volume) (Minifors, Infors HT-Basel, Switzerland) containing fresh optimized medium. The culture parameters were set as it follows: pH 7.0 (adjusted with 1.0 N NaOH or HCl), stir rate of 100 rpm, temperature 28 °C and undetectable oxygen. The anaerobic condition was achieved by purging sterile nitrogen and in fresh medium until the oxygen sensor reading reached zero. The medium was then purged with N_2O for 15 minutes.

Isolation of BMs

At the end of the growth period in bioreactor, cells were collected by centrifugation at 6100 × *g* at 4 °C for 15 min. The cell pellets were washed and resuspended in 15 mL of HEPES buffer (10 mM). Afterwards, the cells were lysed in ultrasonic cell crusher (VCX 500, Sonics, Newtown, CT, USA) at 40% amplitude, 20 kHz frequency, in 60 cycles of 30 s between intervals of 30 s. The BMs were magnetically concentrated by a neodymium–boron magnet attached to the outside of the tube for 12 h at 4 °C. The crystals were transferred into 1.5 mL polypropylene tubes and resuspended in HEPES buffer (10 mM) with NaCl (200 mM). The crystals were then washed in an ultrasonic bath (Branson 2200, Emerson, Rochester, NY, USA) for 4 cycles of 30 min, with magnetic concentration and exchange of the buffer at each cycle. The washing efficiency and conservation of the BM membrane were verified by transmission electron microscopy.

Transmission electronic microscopy

Suspensions of pure and functionalized BMs were added on Formvar-coated copper grids and vacuum-dried. Samples were observed in a transmission electron microscope (FEI Morgagni, Hillsboro, OR, USA) operating at 80 kV in magnifications of 16 000 and 42 000 times.

Size measurements of BMs

Measurements of length and width of the BMs used in this study as well as evaluation of the membrane thickness surrounding the BMs before and after functionalization were performed using the iTEM (Olympus, Tokyo, Japan) program. The length and width of the crystals were obtained from the measurements of maximum diameter and minimum diameter, respectively. Graphs and statistical analyzes of the data were carried out with the aid of the Prism 5.0 program (GraphPad Software, San Diego, CA, USA).

Preparation of functionalized nanoparticles

The functionalization of the isolated BMs with AmB were performed by an adapted method.[2] Briefly, 100 μg of BMs were added to 100 μL of 0.1 M phosphate buffer (pH 7.4). GA was added for crosslinking at different final concentrations (0.2, 3.5 and 12.5% v/v). AmB dispersed in DMSO was then added to a final concentration of 125 μg mL^{-1}. The system was subjected to 5 cycles of 10 minutes sonication at 60 W in a sonicator bath, at 10 min intervals under ice bath cooling. The same procedure was performed with BMs pre-treated with PLL at different concentrations (0.1, 0.01 and 0.001‰). At the end, the functionalized BMs were magnetically concentrated and the supernatant was removed and used to estimate the capture efficiency

of AmB by absorbance at 410 nm. The loading of drug was also calculated from the amount of drug captured and the mass of magnetite added to the functionalization reaction. Aliquots of them were also submitted to transmission electron microscopy observation, as previously described. The experiments were performed in triplicate and the capture efficiency displayed by each system was compared statistically by the ANOVA test using the Prism 5.0 program. The functionalized nanoparticles were vacuum dried and stored frozen at −20 °C until used for experiments.

Fourier transform infrared spectroscopy

Lyophilized samples of approximately 1 mg were placed in direct contact with the infrared attenuated total reflection (ATR) diamond crystal of an IRPrestige-21 Spectrometer (Shimadzu, Kyoto, Japan). All preparations were analysed in the wavenumber range of 3000 to 500 cm^{-1} by co-adding 80 scans with a resolution of 1 cm^{-1}.

Ultraviolet-visible spectrometry

The preparations showing the highest drug loadings were analysed according to the Identity Test described in The International Pharmacopoeia.[25] The protocol has been slightly adapted to allow the analysis of magnetic nanoparticles. Briefly, lyophilized samples of 100 μg were treated with methanol for the extraction of membrane-bound material. The extracts were, then, analysed in a UV-1800 (Shimadzu, Kyoto, Japan) spectrophotometer operating in scanning mode in the wavelength range of 300–450 nm. A negative control was performed using raw BMs. A positive control with free AmB was performed according to the Pharmacopoeia without adaptations.

Zeta potential

The zeta potential of resuspended nanoparticles in ultrapure water (30 μg mL^{-1}) was measured on a Zeta Analyzer (ZetaPlus, Brookhaven Instruments Corp., Holtsville, USA). Ten measurements were performed on each sample and the individual values were used to calculate the mean and standard deviation.

Magnetic hyperthermia

The heating capacity of the BMs in response to the application of AMF was investigated. The analysis was performed on a magnetic induction heating system (DM2-s53, Nanoscale Biomagnetics, Zaragoza, Spain) equipped with an optic fiber temperature probe and vacuum thermal insulation. Suspensions of BMs in PBS (pH 7.4) were transferred to a glass vial (1 mL) at concentrations of 1.2 and 4.8 mg mL^{-1}. The system temperature was stabilized at 22 °C for 8 min and the AMF was applied at a frequency of 307 kHz and magnetic field strength of 200 Oe.

Drug release profile

Three types of conjugates were tested for the released profile of AmB. Basically, BM–PLL–AmB and BM–PLL–GA–AmB complexes were dispersed in PBS and incubated at 37 °C under agitation at 60 rpm.[26] At 5, 10, 20 and 60 minutes, magnetic nanoparticles were magnetically concentrated and a supernatant sample was collected for the determination of AmB in a spectrophotometer (UV 330G, Gehaka, São Paulo, Brazil) at 410 nm. Thereafter, the BMs were redistributed and the PBS volume was restored. To assess the release of AmB from the nanoparticles in response to AMF, the same procedure was performed for supernatant collection and released drug quantification.

Magnetic measurements

The magnetization properties of BMs was investigated at room temperature using a SQUID vibration sample magnetometer (MPMS3, Quantum Design, San Diego, CA, USA). An amount of 13.9 mg of lyophilized BMs were placed inside a gelatin capsule prior to insertion into SQUID sample holder. Measurements were performed at 300 K.

Results & discussion

BM production

BMs were obtained from a culture of *Mv. blakemorei* strain MV-1^T grown in a 5 L bioreactor using medium and operational optimized conditions.[24] Cells were then lysed by sonication and extracted BMs were washed four times using HEPES buffer (10 mM; pH 6.8) before their utilization in the experiments. Size of isolated BMs ($n = 540$) averaged 64.3 ± 0.5 nm in length and 41.6 ± 0.3 nm in width (Fig. S1†) as measured from transmission electron microscopy (TEM) images.

Preparation of functionalized nanoparticles

Although the abundance of phosphatidyl components of BM membrane[11] gives these nanostructures an overall negative charge, other functional groups are present.[5] The functional groups available on the BM surface are those from side chains of amino acid residues making up membrane proteins.[5] The most important for chemical modifications are amino groups, as these groups have been extensively reported in literature[5,10,14] as anchors for covalent binding of functional molecules. The immobilization of drug molecules onto BMs is usually achieved with iminium-forming crosslinkers, like GA.[13] From that knowledge, different concentrations of GA, ranging from 0.2% to 12.5%, were used for the treatment of BM with AmB (BM–GA–AmB) in this work. In addition, polyaminoacids are also promising agents for adsorption of drugs onto these nanoparticles based on charge interactions.[5,10] Thus, BMs were coated with PLL (concentrations ranging from 0.001 to 0.1‰) before treatment with AmB. PLL-coated BMs were also treated with AmB in the presence and absence of GA (BM–PLL–GA–AmB and BM–PLL–AmB, respectively) in the concentration that yielded the best drug capture efficiency (0.1‰ PLL). When applied as the only linking agent, maximum tested concentrations of either GA and PLL returned the most substantial encapsulation efficiency (35.2 ± 3.5% for BM–GA–AmB and 52.7 ± 2.1% for BM–PLL–AmB) and drug loading (15.5 ± 3.1 μg per 100 μg for BM–GA–AmB and 25.3 ± 1.9 μg per 100 μg for BM–PLL–AmB)

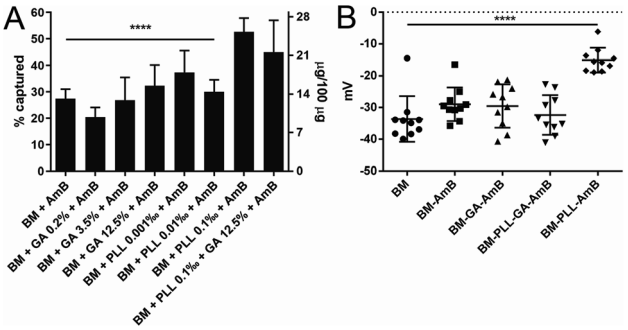

Fig. 1 Encapsulation efficiencies (%) and drug loadings (μg per 100 μg) (A) for different concentrations of GA and PLL in functionalization of BMs. Average zeta potential (B) ($n = 10$) for each preparation. In both analysis PLL and GA were used in the maximum tested concentrations (0.1‰ and 12.5%, respectively). ANOVA tests showed statistically significant difference in efficiencies ($p < 0.0001$, ****).

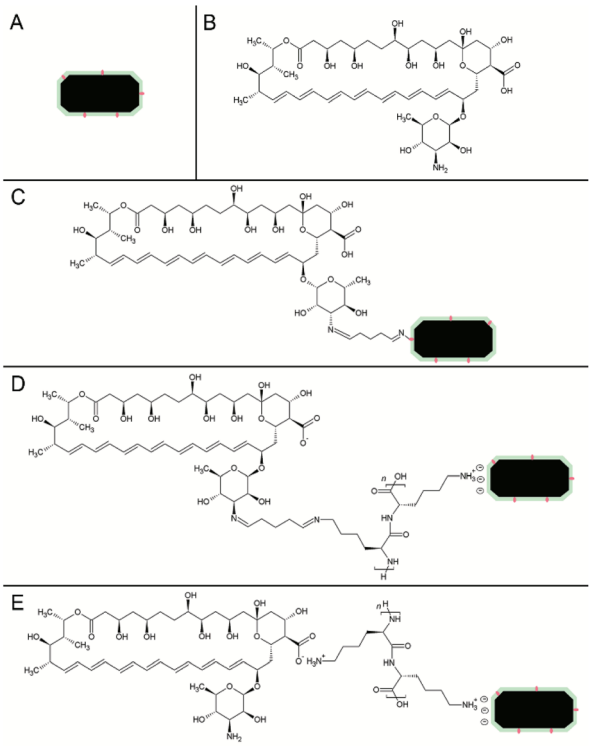

Fig. 2 Representation of free magnetosome (A) and structures of free amphotericin B, with the mycosamine ring at the bottom right, (B) and their conjugates: BM–GA–AmB (C), BM–PLL–GA–AmB (D) and BM–PLL–AmB (E).

(Fig. 1A). Overall, all BMs treated with tested PLL concentrations returned better drug entrapment than those using GA. This is probably due to the fact GA links only to amino groups located in proteins of BM membrane whereas PLL covers BM surface as a whole because of net negative charge provided by phospholipids. No statistically significant difference in encapsulation efficiency and drug loading was found between BM–PLL–AmB (0.1‰ PLL; 45.0 ± 5.4% and 21.6 ± 4.9 μg per 100 μg, respectively) and when both reagents (BM–PLL–GA–AmB) were used (0.1‰ PLL + 12.5% GA; 52.7 ± 2.1% and 25.3 ± 1.9 μg per 100 μg, respectively).

Spectroscopy analyses and chemical structure

The attachment and adsorption of AmB onto BMs were then confirmed using ATR-FTIR spectroscopy analyses (Fig. S2†) and a schematic representation of each preparation is displayed on Fig. 2. Fe–O stretching vibration peaks from magnetite were found in all nanoparticle preparations, ranging from 534 to 564 cm^{-1}. Additionally, the multiplicity of functional groups, including primary amines, has been confirmed in our spectroscopic analysis of raw BMs by the characteristic fingerprint region (1400 to 500 cm^{-1}). The peaks 1643 and 1654 cm^{-1} in BM–GA–AmB and BM–PLL–GA–AmB are assigned to (–CN) vibrations, suggesting the covalent attachment of AmB,[13,23] as illustrated in structures (Fig. 2B and C). The bands ranging from 2943 and 2827 cm^{-1} correspond to $-CH_2$ and $-CH_3$ stretching vibrations of the polyene structure of AmB.[27] In BM–PLL–AmB and BM–PLL–GA–AmB the peak 1622 cm^{-1} is assigned to bending vibration of N–H of amide groups from polyaminoacid backbone of PLL[28] (Fig. 2D and E). Peaks 1528 cm^{-1} in BM–PLL–AmB and BM–PLL–GA–AmB and 1562 cm^{-1} in BM–GA–AmB and AmB correspond to superposed $-NH_2$ bending and $-COO^-$ stretching vibrations from AmB[27] (Fig. 2D and E). Peaks 1383–1401 cm^{-1} in functionalized nanoparticles and AmB correspond to $-COO^-$ stretching and –C=O bending vibrations from AmB.[27] Finally, peaks 1072–1037 cm^{-1} and 1000–1014 cm^{-1} from the same spectra are assigned to pyranose C–O–C stretching and –CH *trans* bending from polyene structure[27] (Fig. 2B–E). These findings support the effective binding of AmB in these preparations and indicate the possible mechanisms in which GA, PLL and AmB interacts with BMs during the preparation of nanoconjugates. When used as the sole linking agent (BM–GA–AmB), GA activates BM surfaces for the covalent binding to molecules containing primary or secondary amino groups through iminium formation.[10,29] When AmB is added to a GA-activated BM suspension, the amino group presents within the mycosamine ring (Fig. 2B) reacts with GA-derived aldehyde group to form a second covalent iminium bond (Fig. 2C). In preparations containing PLL (BM–PLL–AmB and BM–PLL–GA–AmB), the polyaminoacid side chain, which is comprised of a four-carbon chain with a terminal primary amine, is positively charged at neutral pH. Thus, positively charged PLL side chains electrostatically binds to negatively charged phospholipids on the surface of BMs (Fig. 2D and E). The interaction of AmB with PLL in BM–PLL–AmB probably occurs by a hydrogen bond between amine side chain of PLL and carboxyl group present in AmB (Fig. 2E). For BM–PLL–GA–AmB, the BMs are first coated with PLL prior to activation by GA (refer to Preparation of functionalized nanoparticles in Experimental section). In this sense, one of aldehyde groups of GA forms an iminium bond with the aliphatic amino group of the PLL coating (Fig. 2D). Then, the GA-activated complex binds covalently to AmB molecules in a manner analogous to that of BM–GA–AmB.

The adsorption and the stability of AmB attached to the BM–PLL–AmB and BM–PLL–GA–AmB – chosen due to the highest

drug loadings – were investigated through UV-vis spectroscopy. For both preparations, absorption peaks were observed, in crescent intensity order, at 364, 382 and 406 nm (Fig. S3†). The relative intensities between peaks were maintained for the tested nanoformulations, as enforced by the International Pharmacopoeia.[25] This finding corroborates that our synthesized nanoformulations are in accordance to regulatory requirements and meet quality standards for pharmaceutical use.

Membrane thickening measurements

Measurements of membrane thickness of different BMs preparations from TEM images revealed the surface interactions observed after functionalization experiments. All preparations had progressively larger membrane thickness measurements than non-functionalized BMs (Fig. 3 and S4†), with the largest membrane thickness observed for BM–PLL–GA–AmB, when most reagents were attached to the surface of BMs. These results suggest the BM membrane became thicker as more functional moieties were added to its surface. The increase in BM membrane thickness as result of insertion of organic molecules has also been observed in other works.[10,30] It is suggested that such phenomenon could prevent aggregation of BMs caused by interaction between nuclei of single magnetic domain.[31] TEM images also suggested some level of aggregation of nanoparticles, especially in those prepared with GA. This is probably due to unspecific BM–BM crosslinking, which could also explain a lower encapsulation efficiency when using this GA as crosslinking agent.

Zeta potential

The zeta potential was measured to evaluate the dispersive properties of the functionalized nanoparticles. For non-functionalized BMs, a zeta potential of -33.6 ± 2.3 mV was found and agrees with values found for cuboctahedral BM from *Magnetospirillum* strains[14,31] (Fig. 1B). As in other *Magnetospirillum*, BMs in *Mv. blakemorei* strain MV-1^{T} are formed from vesicles internalized from the inner cell membrane,[32] which is composed of negatively charged phospholipids and causes a negative zeta potential. Values between -33 and -28 mV were observed for preparations tested, except BM–PLL–AmB, whose potential was -15.1 ± 3.8 mV (Fig. 1B). Despite the increase of zeta potential value towards zero, all dispersions of tested preparations may be considered at least relatively stable.[33] The change in zeta potential of particles derived from different functionalization methods showed the response of membrane charge to the interaction with the foreign molecules, as corroborated by the encapsulation, membrane thickening and spectroscopic results. This trend has been recently discussed by another work,[29] in which immobilization of anthracycline molecules also leads to significant changes in BM surface charges, as evaluated by zeta potential.

Magnetic characterization

To our knowledge, this is the first time BMs of prismatic shape have its functionalization potential explored. Because of that, magnetic properties for this type of nanoparticle were not

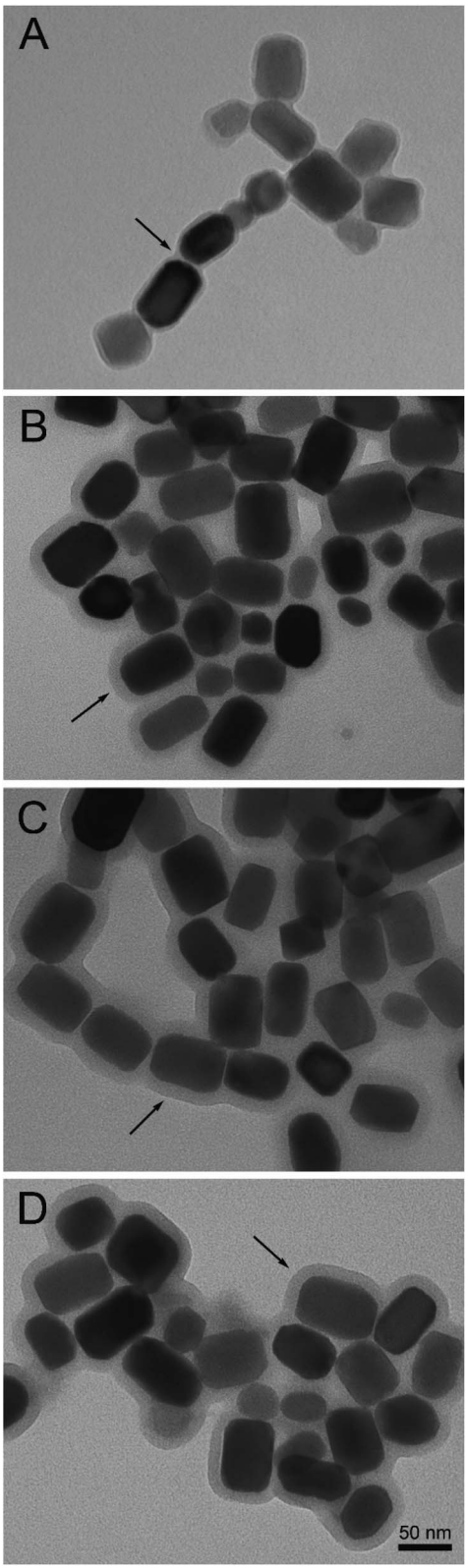

Fig. 3 TEM images of free BMs (A) and its conjugates: BM–GA–AmB (B), BM–PLL–GA–AmB (C) and BM–PLL–AmB (D). Note the membrane thickness increase for different preparations.

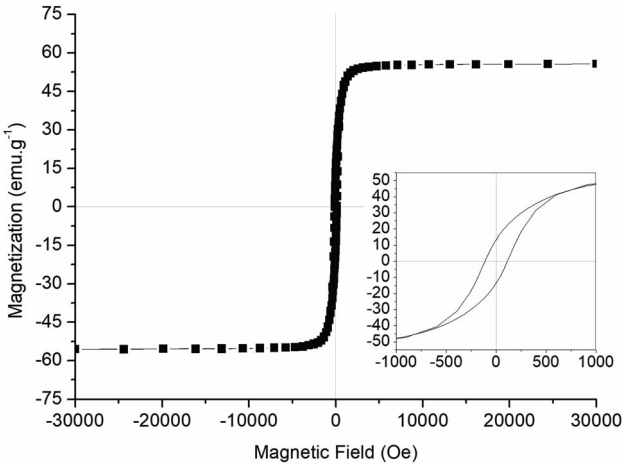

Fig. 4 Magnetization curve of lyophilized magnetosomes from *Mv. blakemorei* strain MV-1^T showing hysteresis loops (inset).

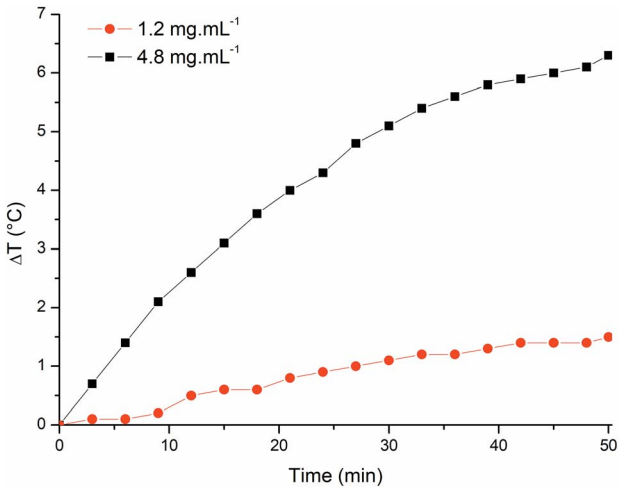

Fig. 5 Heating profile of BM samples (1.2 mg mL^{-1} and 4.8 mg mL^{-1}) subjected to an AMF of 200 Oe and frequency of 307 kHz.

available and had to be evaluated. Magnetization measurements were performed on non-functionalized BMs and presented a behaviour of single magnetic domain particle, as expected (Fig. 4). The values for saturation magnetization and coercivity were 52 emu g^{-1} and 115 Oe. These characteristics and measured values were compatible with the values reported for the cuboctahedral BM of *Magnetospirillum magneticum* strain AMB-1 (ref. 34) and bioinspired greigite nanoparticles.[35] These findings reflect similar applicability potential for the elongated prismatic BMs from *Mv. blakemorei* strain MV-1^T and those nanoparticles already studied.

Heating capacities of suspensions containing 1.2 and 4.8 mg mL^{-1} of magnetite in water were examined under an AMF (field amplitude = 200 Gs; frequency = 307 kHz). The increase in temperature in response to the application of an AMF was the highest (6.3 °C) in the suspension containing the largest amount of magnetite (Fig. 5). When the concentration of magnetite was 1.2 mg mL^{-1}, the temperature increase was also

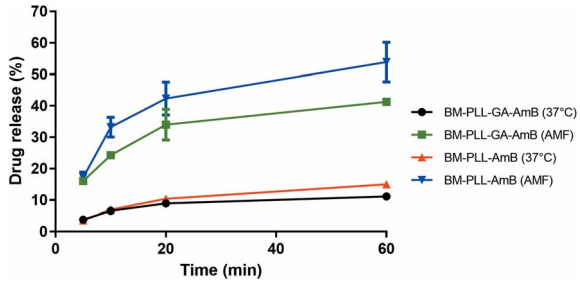

Fig. 6 Cumulative release profile of AmB from different preparations under standard (37 °C) and AMF. PLL and GA were used in the maximum tested concentrations (0.1‰ and 12.5%, respectively).

lower (1.4 °C). The specific absorption rate (SAR) is defined as the rate in which magnetic energy is converted into thermal energy by unit of mass.[36] This property is dependent on mass, shape, size of nanoparticle and on the frequency and the intensity of the applied magnetic field.[36] The SAR values calculated from our experiments are 2.9 and 7.0 W $g_{Fe_3O_4}^{-1}$ for suspensions of BMs with 1.2 and 4.8 mg mL^{-1}, respectively. Both the temperature variation and SAR value achieved here are lower than previously reported values for hyperthermia using BMs.[34,37] However, a similar temperature increase was obtained using similar parameters for AMF-induced heating of BMs from *Magnetospirillum gryphiswaldense* strain MSR-1.[38]

AmB-releasing profile

The amount of AmB released into the medium relative to the amount of drug associated within the nanoparticle was measured in the standard drug release condition (37 °C)[26] and under the application of an AMF. For these experiments, only the preparations with the highest loading of AmB were used (Fig. 6). The release in the standard condition within 1 h was 11.1 ± 0.4% for BM–PLL–GA–AmB and 15.0 ± 1.2% for BM–PLL–AmB. When the suspension was subjected to the AMF, the drug release in the same time interval increased by approximately four times, reaching 41.3 ± 0.5% for BM–PLL–GA–AmB and 53.8 ± 6.2% for BM–PLL–AmB. This increase in the release is attributed to Brown relaxation, which responds for rotation of nanoparticles under AMF, rather than hyperthermia.[36,39] This was also observed in a study in which an increase of about four times of doxorubicin release from cyclodextrin-decorated magnetite nanoparticles was observed without the rise in temperature.[39] In another study, a sharp release of rhodamine B from rhodamine B-fluorescent BMs in response to an AMF occurred in a temperature variation smaller than 2.5 °C.[40]

Conclusions

Here we first demonstrated the functionalization of magnetosomes from *Mv. blakemorei* strain MV-1^T and the decoration of magnetosomes with an antifungal/antiparasitic drug.‡ In our

‡ The results obtained in this study have been registered under the patent number BR1020210056835 held in Brazil.

experiments, it is evidenced that PLL increase binding of AmB onto magnetosomes in the presence and absence of GA. We also demonstrated the controlled drug release from these conjugates with the application of an AMF, which can be useful in localized chemotherapy. These results expand the potential applicability of these magnetic nanoparticles in the treatment of neglected diseases.

Author contributions

All authors contributed to activities necessary to this manuscript. T. C. performed material preparation, data collection and analysis. F. G. analysed the magnetization and heating properties of BMs. T. C., F. G., D. A. B. and F. A. contributed to the study conception and design. All authors read and approved the final manuscript.

Conflicts of interest

There are no conflicts to declare.

Acknowledgements

We acknowledge financial support from the Brazilian agencies Conselho Nacional de Desenvolvimento Científico e Tecnológico (CNPq), Fundação de Amparo à Pesquisa do Estado do Rio de Janeiro (FAPERJ) and Coordenação de Aperfeiçoamento de Pessoal de Nível Superior (CAPES). D. A. B. is supported by U.S. National Science Foundation grant EAR-1423939. Microscopy Facility: Unidade de Microscopia Multiusuário Souto-Padrón & Lins (UniMicro, UFRJ). Optical Spectroscopy Laboratory (Institute of Natural Products Research, UFRJ). We thank Professor Susana Carvajal (Laboratório de Ultraestrutura Celular Hertha Meyer, Institute of Biophysics, UFRJ) for the help in zeta potential analysis.

Notes and references

1 L. H. Reddy, J. L. Arias, J. Nicolas and P. Couvreur, *Chem. Rev.*, 2012, **112**, 5818–5878.
2 M. Estanqueiro, M. H. Amaral, J. Conceição and J. M. Sousa Lobo, *Colloids Surf., B*, 2015, **126**, 631–648.
3 B. I. Kharisov, H. V. R. Dias, O. V. Kharissova, A. Vázquez, Y. Peña and I. Gómez, *RSC Adv.*, 2014, **4**, 45354–45381.
4 E. Alphandery, *Front. Bioeng. Biotechnol.*, 2014, **2**, 5.
5 G. Vargas, J. Cypriano, T. Correa, P. Leão, D. A. Bazylinski and F. Abreu, *Molecules*, 2018, **23**, 2438.
6 R. Uebe and D. Schüler, *Nat. Rev. Microbiol.*, 2016, **14**, 621–637.
7 B. H. Lower and D. A. Bazylinski, *J. Mol. Microbiol. Biotechnol.*, 2013, **23**, 63–80.
8 A. Arakaki, H. Nakazawa, M. Nemoto, T. Mori and T. Matsunaga, *J. R. Soc., Interface*, 2008, **5**, 977–999.
9 J. R. Lloyd, J. M. Byrne and V. S. Coker, *Curr. Opin. Biotechnol.*, 2011, **22**, 509–515.
10 J. Sun, Y. Li, X. J. Liang and P. C. Wang, *J. Nanomater.*, 2011, **469031**, 1–13.
11 T. Yoshino, H. Hirabe, M. Takahashi, M. Kuhara, H. Takeyama and T. Matsunaga, *Biotechnol. Bioeng.*, 2008, **101**, 470–477.
12 T. Honda, T. Tanaka and T. Yoshino, *Biomacromolecules*, 2015, **16**, 3863–3868.
13 J. B. Sun, J. H. Duan, S. L. Dai, J. Ren, L. Guo, W. Jiang and Y. Li, *Biotechnol. Bioeng.*, 2008, **101**, 1313–1320.
14 Q. Deng, Y. Liu, S. Wang, M. Xie, S. Wu, A. Chen and W. Wu, *Materials*, 2013, **6**, 3755–3763.
15 F. Guan, X. Li, J. Guo, G. Yang and X. Li, *Int. J. Nanomed.*, 2015, **10**, 6919–6930.
16 Q. Dai and W. Wu, *Int. J. Nanomed.*, 2015, 1387–1397.
17 J. J. Torrado, R. Espada and M. P. Ballesteros, *J. Pharm. Sci.*, 2008, **97**, 2405–2425.
18 H. Van De Ven, C. Paulussen, P. B. Feijens, A. Matheeussen, P. Rombaut, P. Kayaert, G. Van Den Mooter, W. Weyenberg, P. Cos, L. Maes and A. Ludwig, *J. Controlled Release*, 2012, **161**, 795–803.
19 C. A. Saldanha, M. P. Garcia, D. C. Iocca, L. G. Rebelo, A. C. O. Souza, A. L. Bocca, M. d. F. M. Almeida Santos, P. C. Morais and R. B. Azevedo, *PLoS Neglected Trop. Dis.*, 2016, **10**, 1–18.
20 R. Fernández-García, E. de Pablo, M. P. Ballesteros and D. R. Serrano, *Int. J. Pharm.*, 2017, **525**, 139–148.
21 S. Zaioncz, N. M. Khalil and R. M. Mainardes, *Curr. Pharm. Des.*, 2017, **23**, 509–521.
22 M. Saqib, A. S. A. Bhatti, N. M. Ahmad, N. Ahmed, G. Shahnaz, N. Lebaz and A. Elaissari, *Nanomaterials*, 2020, **10**, 1152.
23 K. Niemirowicz, B. Durnaś, G. Tokajuk, K. Głuszek, A. Z. Wilczewska, I. Misztalewska, J. Mystkowska, G. Michalak, A. Sodo, M. Wątek, B. Kiziewicz, S. Góźdź, S. Głuszek and R. Bucki, *Nanomedicine*, 2016, **12**, 2395–2404.
24 K. T. Silva, P. E. Leão, F. Abreu, J. A. López, M. L. Gutarra, M. Farina, D. A. Bazylinski, D. M. G. Freire and U. Lins, *Appl. Environ. Microbiol.*, 2013, **79**, 2823–2827.
25 *The International Pharmacopoeia*, 8th edn, https://digicollections.net/phint/2018/index.html, accessed May 2019.
26 P. Legrand, M. Chéron, L. Leroy and J. Bolard, *J. Drug Targeting*, 1997, **4**, 311–319.
27 M. Gagoś and M. Arczewska, *Biochim. Biophys. Acta, Biomembr.*, 2010, **1798**, 2124–2130.
28 E. Alphandéry, A. Idbaih, C. Adam, J. Y. Delattre, C. Schmitt, F. Guyot and I. Chebbi, *Biomaterials*, 2017, **141**, 210–222.
29 Y. Geng, J. Wang, X. Wang, J. Liu, Y. Zhang, W. Niu, A. Basit, W. Liu and W. Jiang, *Nanomedicine*, 2019, **14**, 1663–1680.
30 F. Mickoleit, C. B. Borkner, M. Toro-Nahuelpan, H. M. Herold, D. S. Maier, J. M. Plitzko, T. Scheibel and D. Schüler, *Biomacromolecules*, 2018, **19**, 962–972.
31 J. Xu, J. Hu, L. Liu, L. Li, X. Wang, H. Zhang, W. Jiang, J. Tian, Y. Li and J. Li, *Front. Microbiol.*, 2014, **5**, 4–11.
32 F. Abreu, A. A. Sousa, M. A. Aronova, Y. Kim, D. Cox, R. D. Leapman, L. R. Andrade, B. Kachar, D. A. Bazylinski and U. Lins, *J. Struct. Biol.*, 2013, **181**, 162–168.
33 S. Bhattacharjee, *J. Controlled Release*, 2016, **235**, 337–351.

34 M. Timko, A. Dzarova, J. Kovac, A. Skumiel, A. Józefczak, T. Hornowski, H. Gojzewski, V. Zavisova, M. Koneracka, A. Sprincova, O. Strbak, P. Kopcansky and N. Tomasovicova, *J. Magn. Magn. Mater.*, 2009, **321**, 1521–1524.
35 M. Feng, Y. Lu, Y. Yang, M. Zhang, Y. J. Xu, H. L. Gao, L. Dong, W. P. Xu and S. H. Yu, *Sci. Rep.*, 2013, **3**, 1–6.
36 V. N. Nikiforov and E. Y. Filinova, in *Magnetic Nanoparticles*, ed. S. P. Gubin, Wiley-VCH, 2009, pp. 393–455.
37 E. Alphandéry, S. Faure, L. Raison, E. Duguet, P. A. Howse and D. A. Bazylinski, *J. Phys. Chem. C*, 2011, **115**, 18–22.
38 S. Mannucci, L. Ghin, G. Conti, S. Tambalo, A. Lascialfari, T. Orlando, D. Benati, P. Bernardi, N. Betterle, R. Bassi, P. Marzola and A. Sbarbati, *PLoS One*, 2014, **9**, 108959.
39 E. C. D. S. Santos, A. Watanabe, M. D. Vargas, M. N. Tanaka, F. Garcia and C. M. Ronconi, *New J. Chem.*, 2018, **42**, 671–680.
40 E. Alphandéry, D. Abi Haidar, O. Seksek, F. Guyot and I. Chebbi, *Nanoscale*, 2018, **10**, 10918–10933.